JOURNAL OF MECHANICAL ENGINEERING AND SCIENCES (JMES)
ISSN: 2289-4659 e-ISSN: 2231-8380
VOL. 14, ISSUE 3, 7269 – 7281
DOI: https://doi.org/10.15282/jmes.14.3.2020.26.0571

ORIGINAL ARTICLE

Numerical analysis and explore of asymmetrical fluid flow in a two-sided lid-driven cavity

E.A. Azzouz[1,*] and S. Houat[2]

[1] Institute of Maintenance and Industrial Safety, University Mohammed Ben Ahmed Oran 2, Oran, Algeria
[2] MSMPT Group, MNEPM Laboratory University of Abdelhamid IbnBadis of Mostaganem, Mostaganem, Algeria

ABSTRACT – The two-dimensional asymmetrical flow in a two-sided lid-driven square cavity is numerically analyzed by the finite volume method (FVM). The top and bottom walls slide in parallel and antiparallel motions with various velocity ratio ($U_T/U_b=\lambda$) where $|\lambda|=2$, 4, 8, and 10. In this study, the Reynolds number Re_1 = 200, 400, 800 and 1000 is applied for the upper side and Re_2 = 100 constant on the lower side. The numerical results are presented in terms of streamlines, vorticity contours and velocity profiles. These results reveal the effect of varying the velocity ratio and consequently the Reynolds ratio on the flow behaviour and fluid characteristics inside the cavity. Unlike conventional symmetrical driven flows, asymmetrical flow patterns and velocity distributions distinct the bulk of the cavity with the rising Reynolds ratio. For $\lambda>2$, in addition to the main vortex, the parallel motion of the walls induces two secondary vortices near the bottom cavity corners. however, the antiparallel motion generates two secondary vortices on the bottom right corner. The parallel flow proves affected considerably compared to the antiparallel flow.

ARTICLE HISTORY
Revised: 09th Apr 2020
Accepted: 19th Apr 2020

KEYWORDS
Two-sided lid-driven cavity; asymmetrical driving; finite volume method; analysis flow solutions

INTRODUCTION

Fluid dynamics in bounded cavities is technically and scientifically a fundamental problem in the field of fluid mechanics. In addition, it has received important attention over many years not only to its simple geometry, but also to the practical importance of the subject in order to explore the arising physical phenomena such as vortex dynamics, hydrodynamic stability, and flow bifurcation, etc. The flow in lid-driven cavities provides physical insights and valuable experimentation guidance for many engineering applications including short-dwell coating process [1], meniscus roll coating process and polymer melts [2], mixing processes [3, 4], drying chambers [5], and flow over sollar collectors with wind barriers.

The well-known problem one-sided lid-driven cavity has long been an ideal benchmarking example to test various numerical codes. The case where the flow is induced by the tangential motion of the top lid of the cavity was first initiated numerically and analytically by Burggraf [6] for a cavity with unit aspect ratio, and numerically with the famous work by Ghia et al. [7]. Also, a set of experiments were conducted for cavities with various spanwise aspect ratios [8-10]. Idris et al. [11] simulated the fluid flow inside a shallow semi-ellipse lid-driven cavity. Recently, numerical investigations of mixed convection of fluid flow inside a lid-driven square cavity with arc-shaped moving wall [12], micropolar fluid in a lid-driven triangular cavity [13, 14], and micropolar fluid in a right angle triangular cavity [15, 16] have been done. Their results indicate that the wall movement is one of the factors affecting the flow and heat transfer inside the cavity.

Inspired by the evolution of the Shear Layers Flow, flow arising in rectangular containers, and instability process, the traditional one-sided lid-driven cavity flow was followed by the case of two-sided lid-driven cavity flow by Kuhlmann et al. [17]. The generalized flow is induced due to the tangential motion of the two facing walls either in the same direction (parallel wall motion) or in the opposite direction (antiparallel wall motion). Experimental and numerical investigation have been performed to study two- and three-dimensional flows in a two-sided lid-driven cavity with antiparallel wall motion [17]. As a consequence, they found that the basic two-dimensional flow is not always unique, it depends on the cavity aspect ratio and the Reynolds number. An additional two-dimensional flow exists for the same range of parameters with a flow pattern that resembles a cat's eye. With an increase of the Reynolds number, the cat's eye flow is developed into a strongly three-dimensional cellular flow. Furthermore, Kuhlmann et al. [18] found that the transition to a cat's eye flow happens when the strain rate is dominated in the cavity compared to the rotation rate and the type of instability is similar to those in instability of elliptic stagnation point. Albensoeder et al. [19] Numerically investigated the flow in a two-sided lid-driven cavity where they could identify the region of no uniqueness of two-dimensional steady flow in the aspect ratios and Reynolds numbers. Seven steady solutions were obtained for antiparallel wall motion and five steady solutions for parallel wall motion. Based on the linear stability analysis technique, the stability of multiple two-dimensional steady solutions of such a flow and heat transfer has been inspected by Luo and Yang [20]. Besides, Chen et al. [21-23] numerically studied the stability of two-dimensional solution manifold when the induced flow was respectively two-sided parallel motion, tow-sided antiparallel motion, and four-sided lid motion. The authors illustrated the evolution of the bifurcation diagrams and the existent ranges of stable flow in terms of different aspect ratios and Reynolds numbers.

*CORRESPONDING AUTHOR | E.A.Azzouz | ✉ aminazouz31@yahoo.com

Recently, the efficiency of the finite difference method (FDM), higher-order compact scheme (HOC), and lattice Boltzmann method (LBM) have been respectively employed [24-26]. Through this difference, multiple stable solutions for double-sided lid-driven cavity problem was masterfully investigated. Accordingly, the previously listed studies display the possibility of multiple solutions in two-sided lid-driven cavity, the obtained non-unique two-dimensional flows are highly dependent upon the cavity aspect ratios and Reynolds numbers, while the linear stability analysis was performed as in [17, 18, 20-23] to determine whether the achieved solutions are stable or not.

On the other hand, the two-sided cavity flow problem was also studied in terms of simplicity and was often applied to examine unique steady flow solutions. One of the earliest works was done by Oztop and Dagtekin [27] to investigate the flow and heat transfer in a two-sided lid-driven differentially heated square cavity for parallel and two-configuration antiparallel wall motion. They figured out that the fluid flow and heat transfer are affected by the Richardson number and the direction of the wall's movement. For the case of the forced convection dominated (Ri <1), They found that the fluid flow is symmetric and the heat transfer is enhanced for the two-configuration of antiparallel wall motion. However, the fluid flow becomes asymmetric and the heat transfer is reduced for parallel wall motion. Perumal and Dass [28, 29] respectively presented numerical studies by the FDM and the LBM for a two-sided lid-driven square cavity flows with parallel and antiparallel wall motion and Reynolds number up to 2000. Their results determine fluid proprieties and flow patterns that have revealed a good consistency between the two numerical codes. Perumal [30] examined the two-dimensional steady flow in a two-sided deep cavity for Reynolds numbers ranges from 100 to 2000 with aspect ratios that also range from 2 to 5. The formation of different vortices and flow structures influenced by various aspect ratios (AR) and Reynolds numbers were studied by the finite difference method for parallel and antiparallel wall motion. It is noted that as AR increases, the number of primary vortices increases and the direct percolation of the flow is not significantly affected by the moving lids. Marković et al. [31] performed a numerical simulation of two-sided lid-driven flow inside a staggered cavity by using the commercial software ANSYS FLUENT. Fundamentally, in antiparallel wall motion, their results show symmetrical and asymmetrical steady flow patterns for the variety of Re ranges from 50 to 1000, while the obtained steady solutions for parallel wall motion show only asymmetrical flow patterns for the whole range of Re. Munir et al. [32] applied a third-order upwind compact finite difference scheme to investigate steady two-dimensional flow in a two-sided lid-driven square cavity for Reynolds number up to 2000. A free shear layer has been seen horizontally mediate the two primary eddies when the driving is parallel. For antiparallel driving of the two facing walls, only a single primary eddy appears in the bulk of the cavity. However, two secondary eddies could be seen clearly when Re increased beyond 400.

Sidik and Razali [33] explored the fluid flow which is driven by two parallel moving walls in a square cavity with different speed ratios varies from 0 to 1, and Reynolds number ranges from 100 to 1000 with the LBM. They showed that the flow configuration inside the cavity is continuously and asymmetrically developed as a result of the successive change in velocity ratio and Reynolds numbers. Ismael et al. [34] studied the mixed convection in a two-sided lid-driven square cavity with a partial slip for parallel and antiparallel wall motion. Their results under the conditions of Richardson number Ri (0.01-100) and partial slip parameter S (0-∞) showed that the flow and heat transfer are sensitive to the direction of the moving walls, the Richardson number, and the slip parameter. They found that there are critical values of partial slip parameter at which the convection is declined. Ismail et al. [35] investigated the mixed convection in two-sided lid-driven trapezoidal cavities with parallel and antiparallel wall motion. They showed that both the direction of the moving walls and their inclination angle play a key role on the flow comportment and heat transfer inside the cavity. Lately, Arun and Satheesh [36] explored the two-dimensional steady flow in a cavity with two-moving walls in the same and opposite directions. The numerical results have been presented for Reynolds number $100 \leq Re \leq 5000$, and aspect ratio AR=1, 2 and 5. The detailed flow is visualized in the form of different streamline patterns, velocity profiles, and pressure contours. It is found that for AR=4, there is no secondary vortex formed when the driving is parallel. However, the antiparallel wall motion showed small secondary vortex formed in the vicinity of Re=5000. Numerical study of the flow in a two-sided lid-driven square cavity via using a time-dependent compact scheme with stream-function velocity formulation has been investigated by Karmakar and Pandit [37]. For parallel and antiparallel motion of the two facing walls, different vortex structures and free shear layers were revealed at different time stations when Reynolds number is equal to 1000.

Regardless the study of the flow multiplicity, one can note from above that the vast majority of studies and researches of a unique solution have been discussed only in symmetrical driving, in which the absolute values of the wall-imposed velocities are equal. So far there are few studies report the assessment of asymmetrical flow driving in a two-sided lid-driven cavity however they were either restricted to investigate the fluid flow for only parallel wall motion [33] or intended to study the mixed convection where the flow is under the effect of both moving walls and temperature gradients [34]. For this purpose, an effort has been made to report a systematic examination of unique stable flow in a two-sided lid-driven square cavity, the focus is on asymmetrical driving of the two moving lids when absolute various velocity ratios (λ) are suggested within the range from 2 to 10 for Re=100 in the bottom. Results include fluid characteristics in the vortices center, stream function, vorticity contours, and velocity profiles. The asymmetrical flow driving was explored and the effects of various velocity ratios were visualized with the Finite Volume Method (FVM).

PROBLEM STATEMENT & GOVERNING EQUATIONS

A two-dimensional double-sided facing lid-driven square cavity is considered with a fluid set into motion. The upper and lower walls move independently and simultaneously in the right direction for parallel wall motion. For antiparallel

wall motion, the lower wall is set into the left direction opposite to the upper wall. The two remaining vertical walls are taken to be at rest.

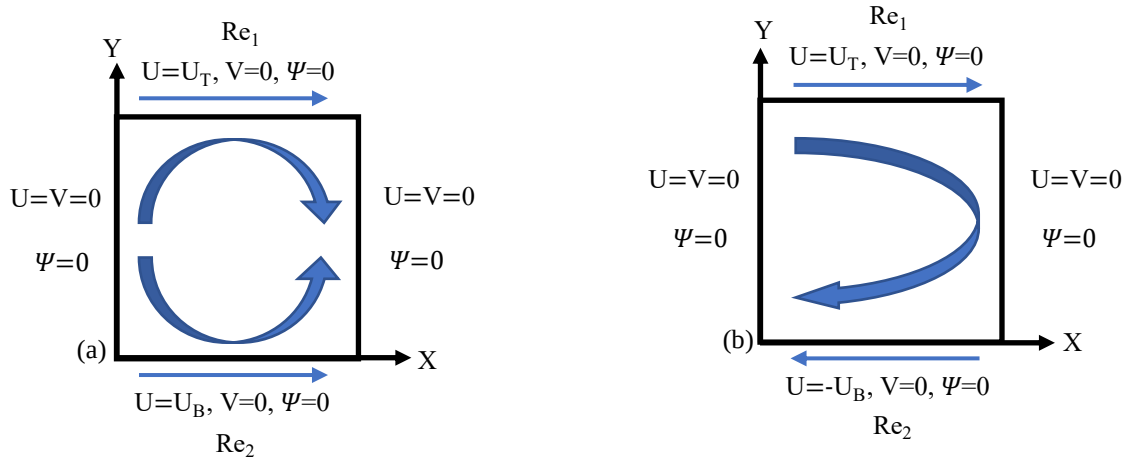

Figure 1. Schematic geometry of the cavity and boundary conditions: (a) parallel wall motion and (b) antiparallel wall motion

Considering the driving is asymmetrical $|Re_1| \neq |Re_2|$, the upper wall is supposed to be induced with different velocities, $U_T = \lambda U_B$, involving a variable velocity ratio ($\lambda = U_T/U_B$), while U_B is kept constant with $Re_2=100$. No-slip conditions are imposed on the fluid overall boundaries. The schematic geometry of the problem under investigation is shown in Figure 1(a) and 1(b). The fluid that is used in the present investigation is assumed to be incompressible and Newtonian, and the flow is considered steady, laminar, and two-dimensional. Dimensionless governing equations of mass Eq. (1) and momentum Eqs. (2, 3) (Navier-Stokes equations) are written through using these assumptions in the Cartesian coordinate system in the following forms:

$$\frac{\partial U}{\partial X} + \frac{\partial V}{\partial Y} = 0 \tag{1}$$

$$U\frac{\partial U}{\partial X} + V\frac{\partial U}{\partial Y} = -\frac{\partial P}{\partial X} + \frac{1}{Re}\left[\frac{\partial^2 U}{\partial X^2} + \frac{\partial^2 U}{\partial Y^2}\right] \tag{2}$$

$$U\frac{\partial V}{\partial X} + V\frac{\partial V}{\partial Y} = -\frac{\partial P}{\partial Y} + \frac{1}{Re}\left[\frac{\partial^2 V}{\partial X^2} + \frac{\partial^2 V}{\partial Y^2}\right] \tag{3}$$

Where $X=x/H$, $Y=y/H$, $U=u/U_T$, $V=v/U_T$, $P=p/\rho U_T^2$ respectively represent dimensionless variables of fluid position in cartesian coordinate, velocity components and pressure. With (H) denotes the physical size of the cavity, (ρ) the fluid density and (μ) the dynamic viscosity, the Reynolds number can be written as:

$$Re_{1,2} = \frac{\rho U_{T,B} H}{\mu} \tag{4}$$

The stream-function (Ψ) and vorticity (ω) could be obtained from velocity components definitions :

$$U = -\frac{\partial \Psi}{\partial Y}, \qquad V = -\frac{\partial \Psi}{\partial X}, \qquad \nabla^2 \Psi = \omega \tag{5}$$

The boundary conditions of the cavity flow are employed in the numerical computation and expressed for parallel and antiparallel wall motion as follow:

(A) On the top wall (Y=1): $U = U_T = \lambda U_B, \quad V = 0, \quad \Psi = 0$ (6)

(B) On the bottom wall (Y=0): $U = |U_B|, \quad V = 0, \quad \Psi = 0$ (7)

(A) On the right wall (X=1): $U = 0, \quad V = 0, \quad \Psi = 0$ (8)

(A) On the left wall (X=0): $U = 0, \quad V = 0, \quad \Psi = 0$ (9)

Conditions (a), (c) and (d) are identical for parallel and antiparallel wall motion. However, the velocity component U in condition (b) respectively causes ($U=U_B$) and ($U=-U_B$) for parallel and antiparallel wall motion. Note that no-slip condition at the non-porous walls yields that the stream-function value vanishes at all boundaries ($\Psi=0$).

NUMERICAL METHOD

The commercial CFD software package ANSYS FLUENT based on the Finite Volume Method (FVM) was used to solve the steady two-dimensional Navier-Stokes equations described by the selected mathematical models in terms of continuity equation Eq. (1) and momentum equations Eq. (2, 3). Thereby, the desired computational cavity domain is subdivided into a finite number of control volumes centroid at every point of a structured hexahedral numerical grid, where the integrated form of the conservation's equations lies. Moreover, a key Gauss' divergence theorem is applied to convert volume integrals into surface integrals. Interpolations schemes are used in this discretization process to deal with different terms which are described by the following characteristics: the second-order upwind scheme was used for the advective terms; central difference scheme [38] for pressure and diffusive terms; Least Squares Cell-based on gradients which are needed for constructing values at the cell face and computing secondary diffusion terms and velocity derivatives; the simple algorithm [39] handles the pressure-velocity coupling. It is worthy to point that no boundary conditions are required for pressure in this model [38].

The resulting system of equations will be a system of linear algebraic equations. Efficient iterative methods involve a point implicit linear equation solver in conjunction with an algebraic multigrid method is used for the solving process. A converged solution was achieved by running the computations when the absolute residual of mass and momentum become less than 10^{-7}.

MESH INDEPENDENT TEST

To choose an optimal mesh for implementation in the present study a grid-sensitivity analysis was used.

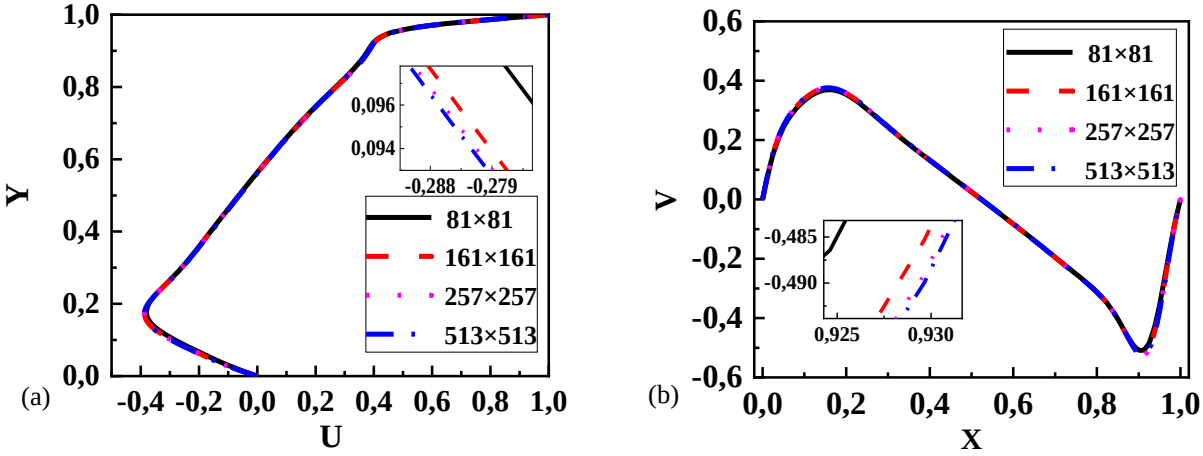

Figure 2. Grid independence test: U- and V-velocity components passing through the vertical centerline (a) and the horizontal centrerline (b) for Re=1000 and various mesh resolution

The U-velocity on the vertical centerline and the V-velocity of the horizontal centerline are displayed in a one-sided lid-driven cavity for Re=1000 with various mesh resolution. The obtained results from this computation are shown in Figure 2(a) and 2(b). It is seen that the velocity curves are very close and the differences are almost marginal, mostly when the grid size exceeds 257×257, in which it becomes less effective on the obtained solutions. Hence, to save time consumption and get more accurate results, an optimal grid of 257×257 with non-equal space is chosen and used for all calculations.

CODE VALIDATION

Stringent tests verification should be performed to confirm the proposed solution method. the popular one-sided lid-driven cavity with unit aspect ratio will be considered for the validation purpose. Therefore, the present numerical results are compared to results obtained from [7] and [40].

Figure 3(a) and 3(b) shows a comparison of U and V components velocity at the vertical and the horizontal centerlines of the cavity, respectively with the obtained results by [7] on a coarse grid of 129×129. As can be seen from velocity curves, a good agreement exists for different Reynolds numbers between the two numerical results.

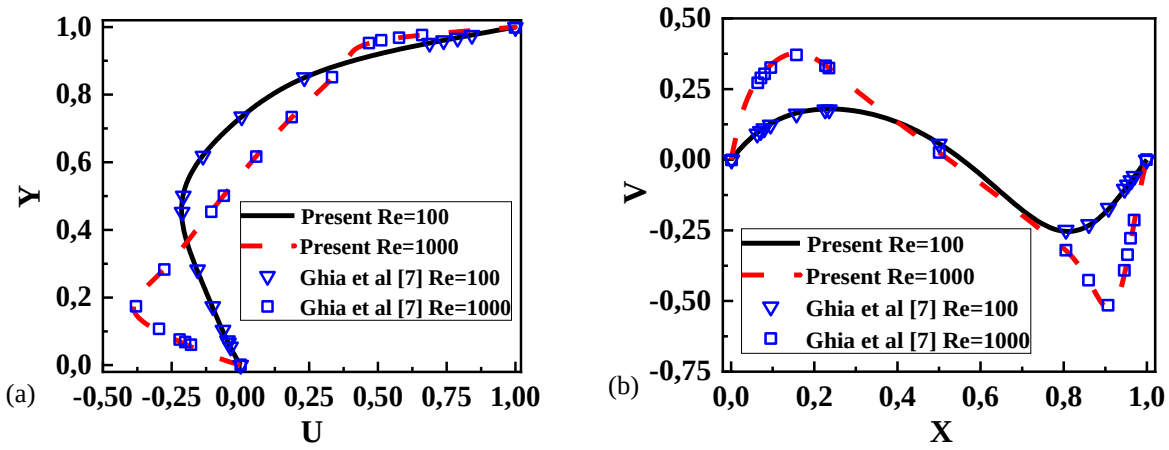

Figure 3. Code validation: U- and V-velocity components passing through the vertical centerline (a) and the horizontal centerline (b) for Re=100 and 1000 compared with [7]

Also, to further support the credibility of the method, values of stream-function (ψ) and vorticity (ω) corresponding to the main primary and the two secondary vortices center are tabulated for Re=1000, and they are also compared with those obtained from [7] and [40] as shown in Table 1. Upon examination of the table, the maximum percentage relative deviation of stream-function and vorticity values for the primary vortex is approximately 0.87% and 0.92%, respectively. The two bottom secondary vortices are identified in a variation lower than 1.20% for stream-function and a relatively higher value for vorticity about 4.13%. Undoubtedly, fluid properties look in fair agreement with the preliminary mentioned data, thereby the present finite volume method stands validated.

Table1. Comparison of stream function-vorticity values for Re=1000 with the results of [7] and [40].

Authors	Grid	Primary vortex		Right secondary vortex		Left secondary vortex	
		Ψ	ω	Ψ	ω	Ψ	ω
Ghia et al. [7]	129×129	-0.117929	2.04968	1.75102E-03	-1.15465	2.31129E-04	-0.36175
Botella et Peyret [40]	160×160	0.1189366	2.067753	-1.729717E-03	-1.109789	-2.334528E-04	-0.3522861
Present	257×257	-0.118969	-2.068799	1.730248E-03	1.108873	2.321085E-04	0.350789

RESULTS & DISCUSSIONS

The investigation of asymmetrical unique flow in a two-sided lid-driven square cavity restricted to the case of parallel wall motion has been addressed [33]. In the light of this study and to further explore the predicted flow asymmetrically induced inside the square cavity, two-dimensional steady numerical results for asymmetrical flow driving in a two-sided lid-driven square cavity for both parallel and antiparallel wall motion are examined through this section. The bottom wall moves with a constant velocity either in the right direction, $U=U_B$ (parallel wall motion), or the left direction, $U=-U_B$ (antiparallel wall motion), obtained through a low fixed Reynolds number equal to $Re_2=100$, while the top wall slides in the right direction with different velocities, $U_T=\lambda U_B$, with respect to various imposed absolute velocity ratios, $|\lambda|=2$, 4, 8 and 10. Besides, Our attention is restricted to this case extension of the published works of symmetrical driving in order to clarify the impact of the velocity ratios (λ) on the arising flow patterns, velocity profiles, and fluid proprieties within the cavity and to provide more benchmarking numerical results for the comparison purpose for future investigations. It is worth mentioning that the main flow structure for results obtained with $Re_2=100$ could be generalized for higher Reynolds numbers (Re_1= 400, 600 and 1000) as the flow essentially reacts with similar trends.

Parallel Wall Motion

Figure 4 depicts stream-function contours obtained for the asymmetrically driven flow in parallel wall motion ($U_T \neq U_B$) for $Re_2=100$ at different velocity ratios ranging from 2 to 10. It is clearly seen that the flow pattern inside the driven cavity is very sensitive to the variation of velocity ratios. At $\lambda=2$, the inducement on the top wall is twice as important as the inducement on the bottom wall. Consequently, the flow pattern is characterized by two main primary counter-rotating vortex one to another. The upper vortex filled the bulk of the cavity with a clockwise rotating while the bottom vortex is confined in the lower part of the cavity occupying less volume than the upper one that rotates in an anticlockwise direction.

For 4≤λ≤10, the main clockwise vortex becomes more powerful, in which it occupies more space inside the cavity. However, the lower vortex is shortened and divided into two individual secondary vortices adjacent to the bottom corners of the cavity with a nearly stagnant region in the middle as a result of the compressing effect of the main upper vortex. The two resulting secondary vortices are anticlockwise rotating. Moreover, with the increased velocity ratio (λ) the asymmetry of the flow gradually increased as it is obvious from the separating shear layer at the junction of the primary vortex with secondary vortices while the centre of the primary vortex moves gradually to be somewhat closer to the geometric cavity center. Furthermore, the centre of two secondary vortices shifts closer to the bottom right and bottom left corners of the cavity. Figure 5 shows vorticity contours for λ=2, 4, 8 and 10 were high vorticity gradients are featured by concentrations.

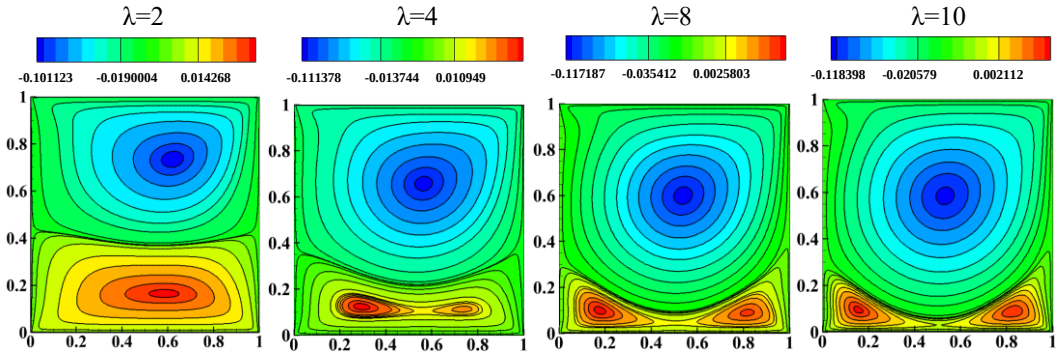

Figure 4. Stream-function contours for differents velocity ratios

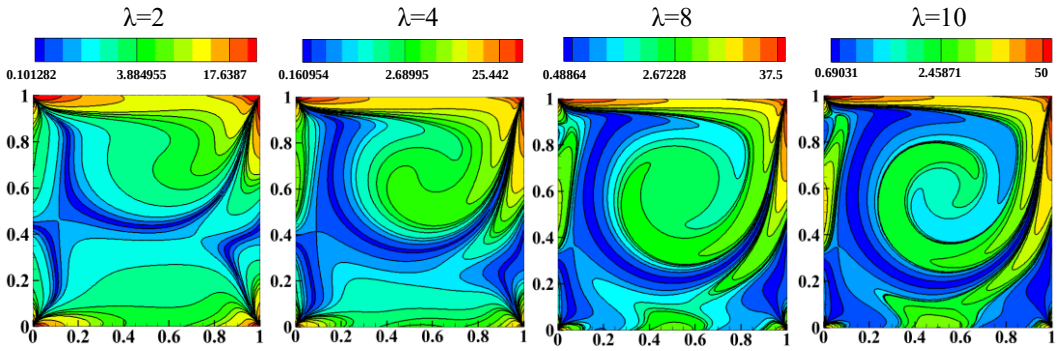

Figure 5. Vorticity contours for differents velocity ratios

Figures 6-9 illustrate the variation of U and V velocities components along the vertical lines (X=0.25, 0.5, 0.75) and the horizontal lines (Y=0.25, 0.5, 0.75), respectively, for Re_2=100 at various velocity ratios, λ= 2, 4, 8 and 10. It is clearly seen that the maximum magnitude of velocity profiles increases continuously with the augmentation of velocity ratios (λ) from 2 up to 10. Moreover, the U-velocity components reached their maximum ($|U_{max}|$) within the cavity along the vertical centerline (X=0.5) below the centre of the cavity in contrary to the case of parallel wall motion with symmetrical driving reveals the fact that the velocity distribution inside the cavity, is highly affected by the separating shear layer strength that is confined to the lower part of the cavity.

The maximum U-velocity component ($|U_{max}|$) along (X=0.75) remains greater than that along (X=0.25). whilst, the maximum value V-velocity component ($|V_{max}|$) is reached within the cavity along the horizontal line (Y=0.75) approximately near the top right corner of the cavity. No longer symmetry exists for velocity profiles.

To provide more clarification and support the numerical results displayed above, the location of the primary and the secondary vortices centre's calculated for λ= 2, 4, 8 and 10 with Re_2=100 are provided in Table 2. Moreover, a comprehensive analysis of the proprieties of the primary and secondary vortices are listed in Table 3 in terms of stream-function and vorticity values at the aforementioned vortices locations (see Table 2).

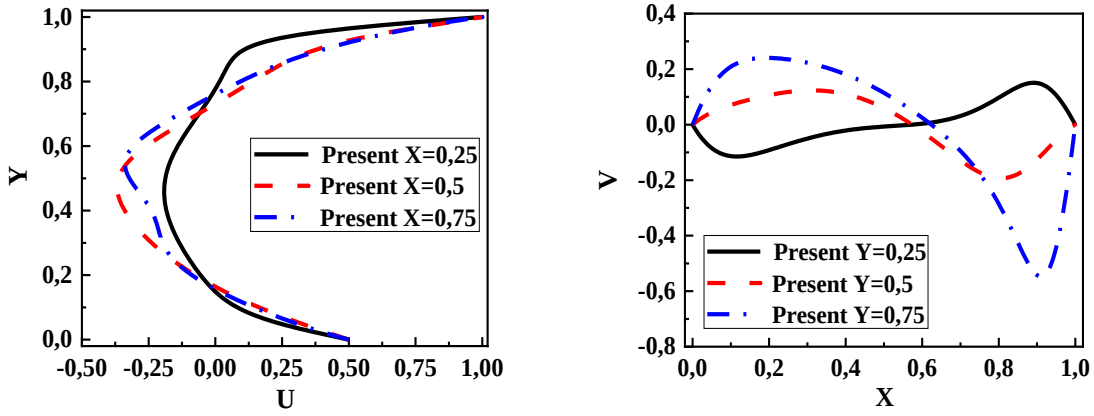

Figure 6. Velocity components profiles for λ=2: (a) horizontal velocity U through the vertical lines (X=0.25, 0.5, 0.75), (b) vertical velocity V through the horizontal line (Y=0.25, 0.5, 0.75)

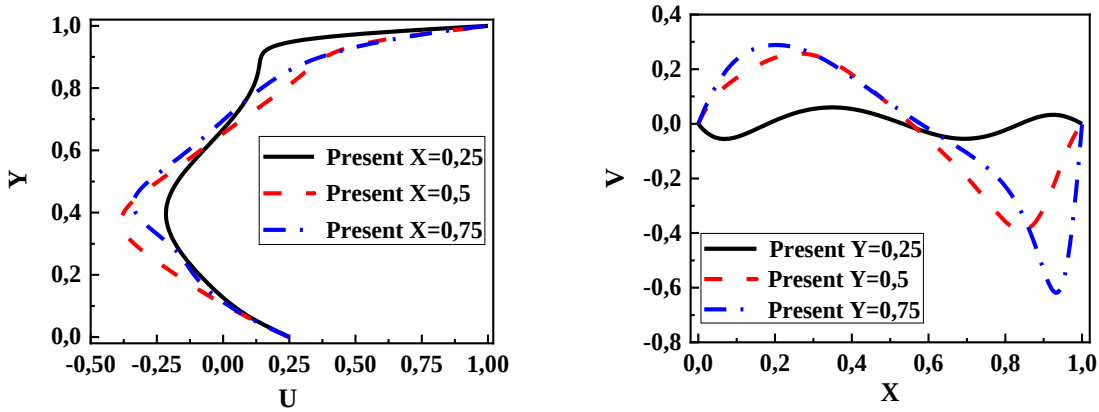

Figure 7. Velocity components profiles for λ=4: (a) horizontal velocity U through the vertical lines (X=0.25, 0.5, 0.75), (b) vertical velocity V through the horizontal line (Y=0.25, 0.5, 0.75)

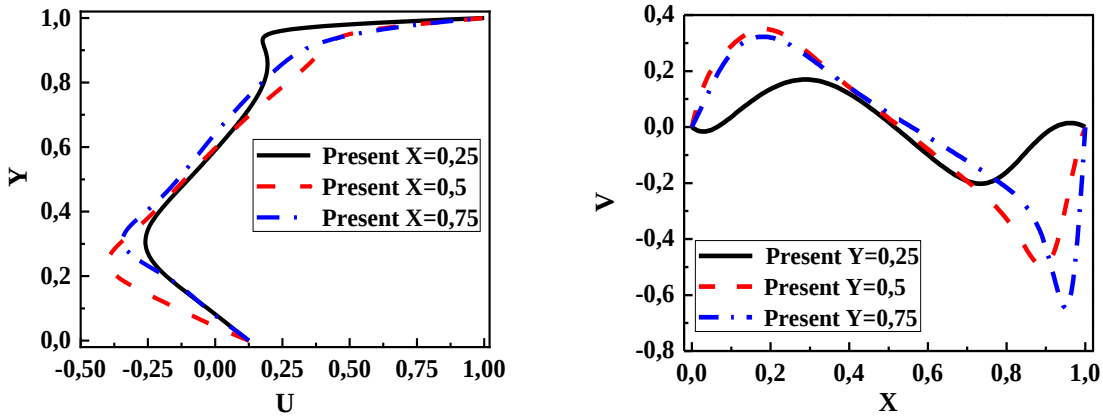

Figure 8. Velocity components profiles for λ=8: (a) horizontal velocity U through the vertical lines (X=0.25, 0.5, 0.75), (b) vertical velocity V through the horizontal line (Y=0.25, 0.5, 0.75)

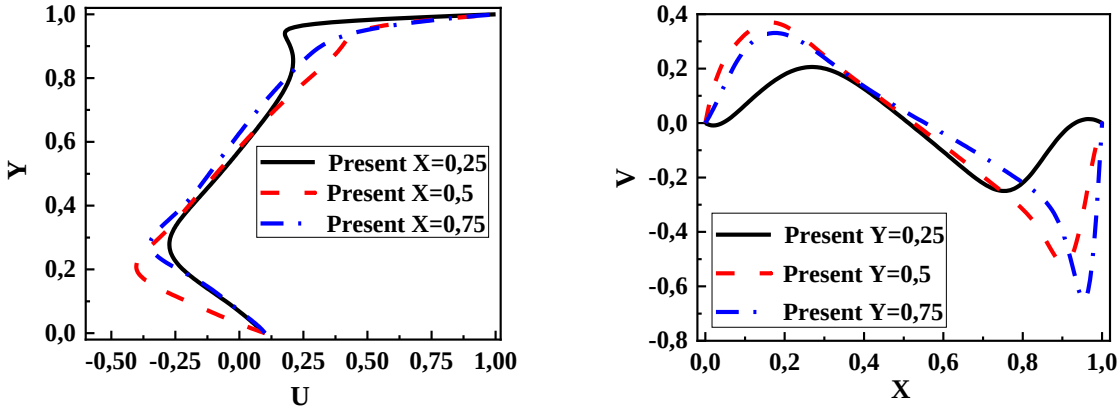

Figure 9. Velocity components profiles for λ=10: (a) horizontal velocity U through the vertical lines (X=0.25, 0.5, 0.75), (b) vertical velocity V through the horizontal line (Y=0.25, 0.5, 0.75)

Table 2. Locations of primary and secondary vortex centre for various velocity ratios

λ	Primary vortex				Secondary vortex			
	Top		Bottom		Bottom left		Bottom right	
	X	Y	X	Y	X	Y	X	Y
2	0.62039	0.7340	0.58658	0.16468	-	-	-	-
4	0.56442	0.65779	-	-	0.29345	0.12391	0.73664	0.11302
8	0.53775	0.60021	-	-	0.17699	0.09991	0.81654	0.09042
10	0.53287	0.58518	-	-	0.15559	0.09588	0.82618	0.08780

Table 3. Stream-function and vorticity values for the primary and secondary vortex

λ	Primary vortex				Secondary vortex			
	Top		Bottom		Bottom left		Bottom right	
	Ψ	ω	Ψ	ω	Ψ	ω	Ψ	ω
2	-0.102416	-3.391378	0.011628	2.492225	-	-	-	-
4	-0.112153	-2.656067	-	-	0.064363	1.859894	0.063030	1.866561
8	-0.118045	-2.252291	-	-	0.005845	1.524924	0.005374	1.423151
10	-0.119218	-2.173113	-	-	0.004535	1.436484	0.004418	1.359763

Antiparallel Wall Motion

Figure 10 depicts stream-function contours obtained in the case when the two horizontal walls are sliding in an opposite direction with different velocities (antiparallel wall motion, $U_{T\neq}$-U_B) for Re_2=100 at various velocity ratios within the range -2≤ λ ≤-10. It is noticeable from this figure that the augmentation of velocity ratios (λ) influences the topology of the flow pattern inside the square cavity. Expectedly, the flow is no longer symmetric about the center of the cavity the fact of being accelerated asymmetrically by a significant amount of motion by the top wall comparing to the bottom wall. At λ=-2, the fluid flow consists of a main vortex that occupies most of the cavity with a clockwise rotating. The centre of the main vortex is somewhat shifted from the geometric centre of the cavity toward the top right side. As λ increases to -4, in addition to the main vortex, a minor anticlockwise vortex starts to appear adjacently to the bottom right corner which tends to grow in size and strength with the increased velocity ratios.

When λ increases to reach -10, a gradual formation of a nearly stagnant region is observed under the minor vortex within which a second secondary vortex start to appear. Whilst, the primary vortex centre is seen to shift gradually towards the bottom to be somewhat near the center of the cavity. Figure 11 shows vorticity contours for λ=-2, -4, -8 and -10 where high vorticity gradients are featured by concentrations as can be seen near the wall's extremities while in central region the vorticity is nearly uniform and small.

To demonstrates the effect of various velocity ratios on velocity profiles inside the cavity, U- and V-velocities components along the vertical lines (X=0.25, 0.5, 0.75) and the horizontal lines (Y=0.25, 0.5, 0.75), respectively, are shown in Figures 12-15 for Re_2=100 and λ=-2,-4, -8 and -10. It is seen that the maximum magnitude of velocity profiles increases continuously with the augmentation of velocity ratios. Furthermore, the range of the maximum U-velocity ($|U_{max}|$) within the cavity is expanded from the bottom wall towards the top wall with the increased velocity ratios.

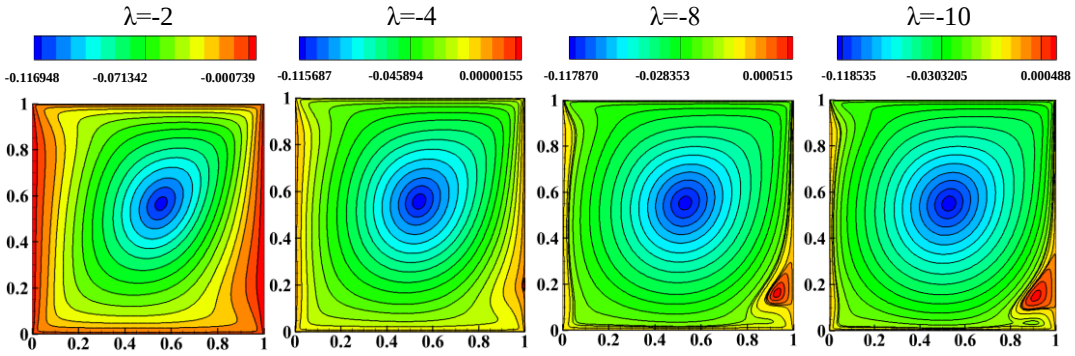

Figure 10. Stream-function contours for differents velocity ratios

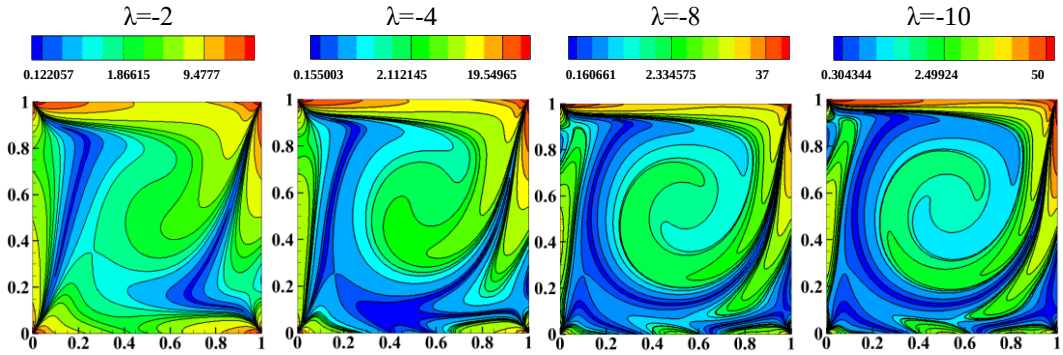

Figure 11. Vorticity contours for differents velocity ratios

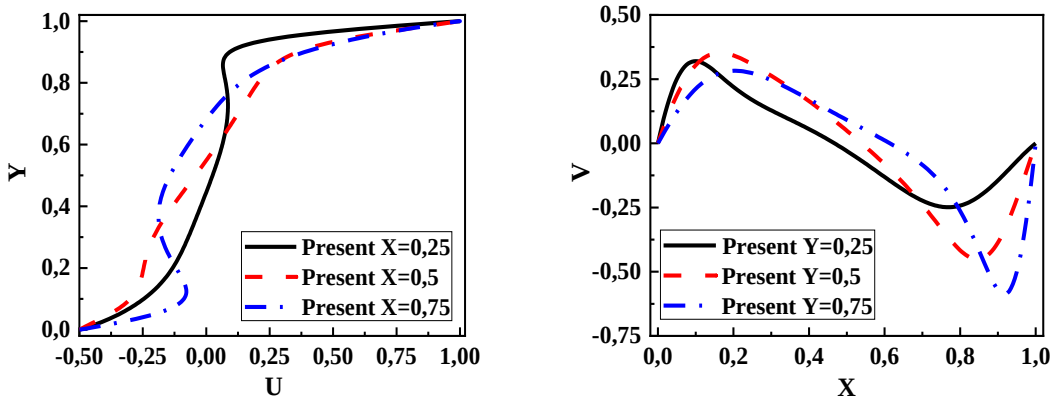

Figure 12. Velocity components profiles for λ=-2: (a) horizontal velocity U through the vertical lines (X=0.25, 0.5, 0.75), (b) vertical velocity V through the horizontal line (Y=0.25, 0.5, 0.75)

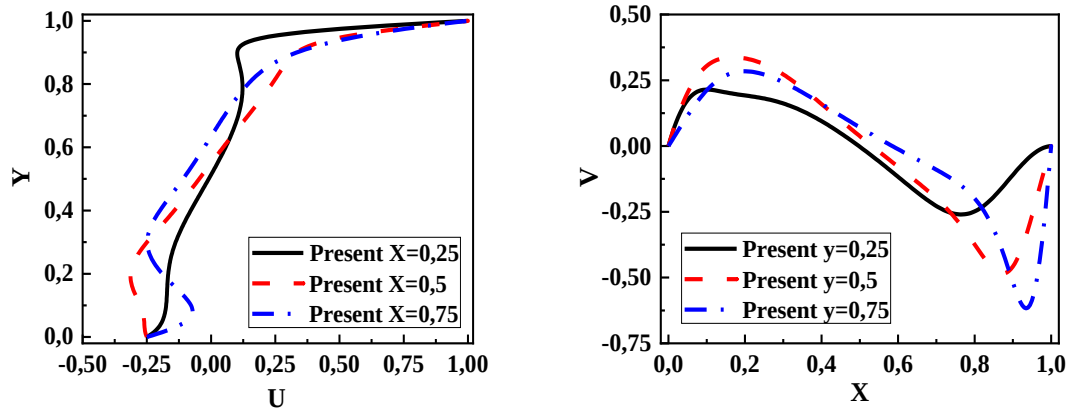

Figure 13. Velocity components profiles for λ=-4: (a) horizontal velocity U through the vertical lines (X=0.25, 0.5, 0.75), (b) vertical velocity V through the horizontal line (Y=0.25, 0.5, 0.75)

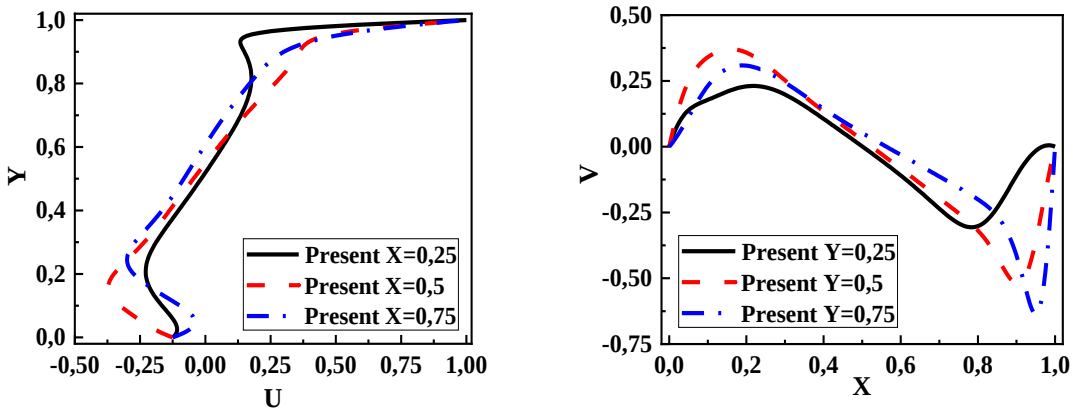

Figure 14. Velocity components profiles for λ=-8: (a) horizontal velocity U through the vertical lines (X=0.25, 0.5, 0.75), (b) vertical velocity V through the horizontal line (Y=0.25, 0.5, 0.75)

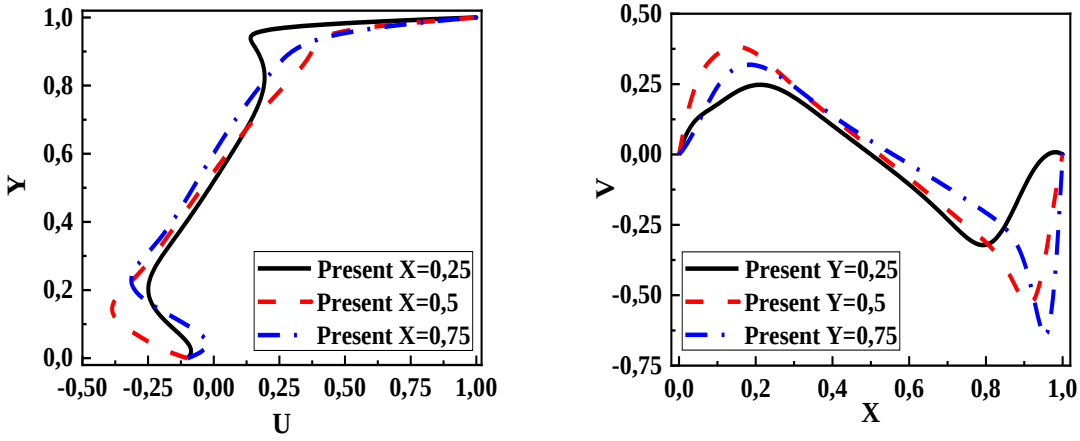

Figure 15. Velocity components profiles for λ=-10: (a) horizontal velocity U through the vertical lines (X=0.25, 0.5, 0.75), (b) vertical velocity V through the horizontal line (Y=0.25, 0.5, 0.75)

Whilst, the maximum V-velocity component ($|V_{max}|$) within the cavity is reached along (Y=0.75) near the top right corner of the cavity.

Tables 4 and 5 provide respectively the locations center and fluid properties in term of stream-function and vorticity values for primary and secondary vortices for Re_2=100 and λ=-2, -4, -8 and -10. These benchmarking results reflect the flow inside the cavity which is more explored. It is worth noting that the circulation rate of the primary vortices remains

relatively large compared to that in secondary vortices for both inducing processes (parallel and antiparallel) as can be seen from vorticity values in Tables 3, 5.

Table 4. Locations of primary and secondary vortex centre for various velocity ratios

λ	Primary vortex		First bottom right secondary vortex		Second bottom right secondary vortex	
	X	Y	X	Y	X	Y
-2	0.55595	0.56593	-	-	-	-
-4	0.54054	0.55746	0.99352	0.20003	-	-
-8	0.53044	0.55286	0.92830	0.16153	-	-
-10	0.52767	0.55053	0.91200	0.14995	0.89908	0.03428

Table 5. Stream-function and vorticity values for the primary and secondary vortex

λ	Primary vortex		First bottom right secondary vortex		Second bottom right secondary vortex	
	Ψ	ω	Ψ	ω	Ψ	ω
-2	-0.117322	-2.115833	-	-	-	-
-4	-0.116165	-2.066008	6.048551E-07	0.076092	-	-
-8	-0.118288	-2.012513	5.793521E-04	0.981028	-	-
-10	-0.119027	-1.998848	9.482300E-04	1.224126	-1.53147E-03	-2.05072

CONCLUSIONS

The second-order Finite Volume Method has been used to simulate two-dimensional flow in a two-sided lid-driven square cavity for parallel and antiparallel wall motion. Unexplored asymmetrical flow ($|Re_1| \neq |Re_2|$) takes attention in this paper in which it greatly demonstrates the employment of various velocity ratios ($2 \leq |\lambda| \leq 10$) to predict the flow behaviour and fluid characteristics inside the driven cavity for $Re_2=100$. Based upon the above discussions we could extract the following:

1. The flow patterns are directly and significantly affected when different velocity ratios cause incitement. No further symmetrical flow exists and an asymmetrical flow arises and evolves continuously with the augmentation velocity ratios.
2. For parallel motion and $\lambda>2$, the flow consists of a clockwise rotating primary vortex occupy the bulk of the cavity and two anticlockwise rotating secondary vortices confined to the lower corners both of which are separated with an arc-shaped shear layer from the primary vortex.
3. For antiparallel motion and $2<|\lambda|<10$, the flow consists of a clockwise rotating primary vortex occupies most of the cavity and an anticlockwise rotating secondary vortex adjacent to the bottom right corner. For $\lambda=-10$, one additional clockwise rotating secondary vortex appears below the first one.
4. Velocity profiles within the cavity were influenced by various velocity ratios and this is evidenced by the increasing magnitudes and asymmetrical distributions. The U velocity components reached their maximum ($|U_{max}|$) along the vertical centerline (X=0.5), this maximum found to be above the separating shear layer for parallel motion and near the bottom wall for antiparallel motion. Whereas, the maximum ($|V_{max}|$) is reached along (Y=0.75) near the top right corner of the cavity.
5. The highest vorticity gradients are obtained near the walls' extremities.

Eventually, a curtain has been taken off on similar flows highly valuable and frequently required in a lot of industrial and engineering applications that also provides a rich multitude of benchmarking information for future investigations.

REFERENCES

[1] Z. Cao and M. N. Esmail, "Numerical study on hydrodynamics of short-dwell paper coaters," *AIChE J.*, vol. 41, no. 8, pp. 1833-1842, 1995, doi: 10.1002/aic.690410802.

[2] P. Gaskell, J. Summers, H. Thompson, and M. Savage, "Creeping flow analyses of free surface cavity flows," *Theor. Comp. Fluid. Dyn.*, vol. 8, no. 6, pp. 415-433, 1996, doi: 10.1007/s001620050025.

[3] C. Leong and J. Ottino, "Experiments on mixing due to chaotic advection in a cavity," *J. Fluid. Mech.*, vol. 209, pp. 463-499, 1989, doi: 10.1017/S0022112089003186.

[4] A. Kouadri, Y. Lasbet, and M. Makhlouf, "High mixing performances of shear-thinning fluids in two-layer crossing channels micromixer at very low Reynolds numbers," *J. Mech. Eng. Sci.*, vol. 13, no. 4, pp. 5938-5960, 2019, doi: 10.15282/jmes.13.4.2019.15.0471.

[5] N. Alleborn, H. Raszillier, and F. Durst, "Lid-driven cavity with heat and mass transport," *Int. J. Heat. Mass. Transf.*, vol. 42, no. 5, pp. 833-853, 1999, doi: 10.1016/S0017-9310(98)00224-5.

[6] O. R. Burggraf, "Analytical and numerical studies of the structure of steady separated flows," *J. Fluid. Mech.*, vol. 24, no. 1, pp. 113-151, 1966, doi: 10.1017/S0022112066000545.

[7] U. Ghia, K. N. Ghia, and C. Shin, "High-Re solutions for incompressible flow using the Navier-Stokes equations and a multigrid method," *J. Comput. Phys.*, vol. 48, no. 3, pp. 387-411, 1982, doi: 10.1016/0021-9991(82)90058-4.

[8] J. Koseff and R. Street, "Visualization studies of a shear driven three-dimensional recirculating flow," *J. Fluids. Eng*., vol. 106, pp. 21-27, 1984, doi: 10.1115/1.3242393.

[9] J. R. Koseff and R. Street, "On end wall effects in a lid-driven cavity flow," *J. Fluids. Eng*., vol. 106, pp. 385-389, 1984, doi: 10.1115/1.3243135.

[10] A. K. Prasad and J. R. Koseff, "Reynolds number and end-wall effects on a lid-driven cavity flow," *Phys. Fluids. A: Fluid. Dyn.*, vol. 1, no. 2, pp. 208-218, 1989, doi: 10.1063/1.857491.

[11] M. Idris, M. Irwan, and N. Ammar, "Steady state vortex structure of lid driven flow inside shallow semi ellipse cavity," *J. Mech. Eng. Sci.*, vol. 2, pp. 206-216, 2012, doi: 10.15282/jmes.2.2012.8.0019.

[12] M. A. Ismael, "Numerical solution of mixed convection in a lid-driven cavity with arc-shaped moving wall," *Eng. Computation.*, vol. 34, pp. 869-891, 2017, doi: 10.1108/EC-11-2015-0368.

[13] N. Ali, M. Nazeer, T. Javed, and F. Abbas, "A numerical study of micropolar flow inside a lid-driven triangular enclosure," *Meccanica.*, vol. 53, no. 13, pp. 3279-3299, 2018, doi: 10.1007/s11012-018-0884-5.

[14] N. Ali, M. Nazeer, T. Javed, and M. Razzaq, "Finite element analysis of bi-viscosity fluid enclosed in a triangular cavity under thermal and magnetic effects," *Eur. Phys. J. Plus.*, vol. 134, no. 1, pp. 1-20, 2019, doi: 10.1140/epjp/i2019-12448-x.

[15] M. Nazeer, N. Ali, and T. Javed, "Numerical simulations of MHD forced convection flow of micropolar fluid inside a right-angled triangular cavity saturated with porous medium: Effects of vertical moving wall," *Can. J. Phys.*, vol. 97, no. 1, pp. 1-13, 2019, doi: 10.1139/cjp-2017-0904.

[16] M. Nazeer, N. Ali, and T. Javed, "Effects of moving wall on the flow of micropolar fluid inside a right angle triangular cavity," *Int. J. Numer. Method. H.*, vol. 28, pp. 2404-2422, 2018, doi: 10.1108/HFF-10-2017-0424.

[17] H. Kuhlmann, M. Wanschura, and H. Rath, "Flow in two-sided lid-driven cavities: non-uniqueness, instabilities, and cellular structures," *J. Fluid. Mech.*, vol. 336, pp. 267-299, 1997, doi: 10.1017/S0022112096004727.

[18] H. Kuhlmann, M. Wanschura, and H. Rath, "Elliptic instability in two-sided lid-driven cavity flow," *Eur. J. Mech. B/Fluids.*, vol. 17, no. 4, pp. 561-569, 1998, doi: 10.1016/S0997-7546(98)80011-3.

[19] S. Albensoeder, H. Kuhlmann, and H. Rath, "Multiplicity of steady two-dimensional flows in two-sided lid-driven cavities," *Theor. Comp. Fluid. Dyn.*, vol. 14, no. 4, pp. 223-241, 2001, doi: 10.1007/s001620050138.

[20] W.-J. Luo and R.-J. Yang, "Multiple fluid flow and heat transfer solutions in a two-sided lid-driven cavity," *Int. J. Heat. Mass. Transf.*, vol. 50, no. 11-12, pp. 2394-2405, 2007, doi: 10.1016/j.ijheatmasstransfer.2006.10.025.

[21] K. Chen, C. Tsai, W. Luo, C. Lu, and C. Chen, "Aspect ratio effect on multiple flow solutions in a two-sided parallel motion lid-driven cavity," *J. Mech.*, vol. 31, no. 2, pp. 153-160, 2015, doi: 10.1017/jmech.2014.51.

[22] K.-T. Chen, C.-C. Tsai, W.-J. Luo, and C.-N. Chen, "Multiplicity of steady solutions in a two-sided lid-driven cavity with different aspect ratios," *Theor. Comp. Fluid. Dyn.*, vol. 27, no. 6, pp. 767-776, 2013, doi: 10.1007/s00162-013-0296-z.

[23] K. T. Chen, C. C. Tsai, and W. J. Luo, "Multiplicity flow solutions in a four-sided lid-driven cavity," in *Applied Mechanics Materials.*, 2013, vol. 368: Trans Tech Publ, pp. 838-843, doi: 10.4028/www.scientific.net/AMM.368-370.838.

[24] T. Lemée, G. Kasperski, G. Labrosse, and R. Narayanan, "Multiple stable solutions in the 2D symmetrical two-sided square lid-driven cavity," *Comput. Fluids.*, vol. 119, pp. 204-212, 2015, doi: 10.1016/j.compfluid.2015.05.022.

[25] C. Prasad and A. K. Dass, "Use of an HOC scheme to determine the existence of multiple steady states in the antiparallel lid-driven flow in a two-sided square cavity," *Comput. Fluids.*, vol. 140, pp. 297-307, 2016, doi: 10.1016/j.compfluid.2016.10.013.

[26] D. A. Perumal, "Lattice Boltzmann computation of multiple solutions in a double-sided square and rectangular cavity flows," *Therm. Sci. Eng. Prog.*, vol. 6, pp. 48-56, 2018, doi: 10.1016/j.tsep.2017.10.009.

[27] H. F. Oztop and I. Dagtekin, "Mixed convection in two-sided lid-driven differentially heated square cavity," *Int. J. Heat. Mass. transf.*, vol. 47, no. 8-9, pp. 1761-1769, 2004, doi: 10.1016/j.ijheatmasstransfer.2003.10.016.

[28] D. A. Perumal and A. K. Dass, "Simulation of Incompressible Flows in Two-Sided Lid-Driven Square Cavities. Part I-FDM," *CFD. Lett.*, vol. 2, pp. 13-24, 2010.

[29] D. A. Perumal and A. K. Dass, "Simulation of Incompressible Flows in Two-Sided Lid-Driven Square Cavities. Part II-LBM," *CFD. Lett.*, vol. 2, pp. 25-38, 2010.

[30] D. A. Perumal, "Simulation of flow in Two-Sided Lid-Driven deep cavities by finite difference method," *JASTFM.*, vol. 6, no. 1, pp. 1-6, 2012.

[31] J. Đ. Marković, N. L. Lukić, J. D. Ilić, B. G. Nikolovski, M. N. Sovilj, and I. M. Šijački, "Using the Ansys Fluent for simulation of two-sided lid-driven flow in a staggered cavity," *Acta. Period. Technol.*, vol. 43, pp. 169-178, 2012, doi: 10.2298/APT1243169M.

[32] A. Munir, M. Rizwan, and A. Shah, "Simulation of incompressible flow in two sided lid driven cavity using upwind compact scheme," *CFD. Lett.*, vol. 5, no. 3, pp. 57-66, 2013.

[33] N. A. Che Sidik and S. A. Razali, "Two-sided lid-driven cavity flow at different speed ratio by Lattice Boltzmann method," in *Applied Mechanics Materials.*, 2014, vol.554: Trans Tech Publ, pp. 675-679, doi: 10.4028/www.scientific.net/AMM.554.675.

[34] M. A. Ismael, I. Pop, and A. J. Chamkha, "Mixed convection in a lid-driven square cavity with partial slip," *Int. J. Therm. Sci.*, vol. 82, pp. 47-61, 2014, doi: 10.1016/j.ijthermalsci.2014.03.007.

[35] M. A. Ismael and A. J. Chamkha, "Mixed convection in lid-driven trapezoidal cavities with an aiding or opposing side wall," *Numer. Heat. Tr A-Appl.*, vol. 68, no. 3, pp. 312-335, 2015, doi: 10.1080/10407782.2014.986001.

[36] S. Arun and A. Satheesh, "Analysis of flow behaviour in a two sided lid driven cavity using lattice boltzmann technique," *Alex. Eng. J.*, vol. 54, no. 4, pp. 795-806, 2015, doi: 10.1016/j.aej.2015.06.005.

[37] H. Karmakar and S. K. Pandit, "Numerical Solutions of Incompressible Viscous Flows in a Double-Lid-Driven Cavity," in *Applied Mathematics*: Springer, 2015, pp. 237-243, doi: 10.1007/978-81-322-2547-8_23.

[38] J. H. Ferziger, M. Perić, and R. L. Street, *Computational methods for fluid dynamics*. Springer, 2002, doi: 10.1007/978-3-642-56026-2.

[39] S. V. Patankar and D. B. Spalding, "A calculation procedure for heat, mass and momentum transfer in three-dimensional parabolic flows," *Int. J. Heat. Mass. Transf.*, vol. 15, pp. 1787-1806, 1972, doi: 10.1016/B978-0-08-030937-8.50013-1.

[40] O. Botella and R. Peyret, "Benchmark spectral results on the lid-driven cavity flow," *Comput. Fluids.*, vol. 27, no. 4, pp. 421-433, 1998, doi: 10.1016/S0045-7930(98)00002-4.